Neuro-Oncology Advances

6(1), vdae024, 2024 | https://doi.org/10.1093/noajnl/vdae024 | Advance Access date 16 February 2024

Preclinical evaluation of the third-generation, bi-steric mechanistic target of rapamycin complex 1-selective inhibitor RMC-6272 in *NF2*-deficient models

Srirupa Bhattacharyya[†], Janet L. Oblinger[†], Roberta L. Beauchamp, Lili Kosa, Francis Robert, Scott R. Plotkin, Long-Sheng Chang, and Vijaya Ramesh

All author affiliations are listed at the end of the article

Corresponding Authors: Vijaya Ramesh, PhD, Department of Neurology and Center for Genomic Medicine, Massachusetts General Hospital, 185 Cambridge Street, Boston, MA 02114, USA (ramesh@helix.mgh.harvard.edu); Long-Sheng Chang, PhD, Center for Childhood Cancer, Nationwide Children's Hospital and Department of Pediatrics, The Ohio State University College of Medicine, 575 Children's Crossroad, Columbus, OH 43215, USA (long-sheng.chang@nationwidechildrens.org).

[†]These authors contributed equally to this work.

Abstract

Background. NF2-associated meningiomas are progressive, highly morbid, and nonresponsive to chemotherapies, highlighting the need for improved treatments. We have established aberrant activation of the mechanistic target of rapamycin (mTOR) signaling in *NF2*-deficient tumors, leading to clinical trials with first- and second-generation mTOR inhibitors. However, results have been mixed, showing stabilized tumor growth without shrinkage offset by adverse side effects. To address these limitations, here we explored the potential of third-generation, bi-steric mTOR complex 1 (mTORC1) inhibitors using the preclinical tool compound RMC-6272.

Methods. Employing human *NF2*-deficient meningioma lines, we compared mTOR inhibitors rapamycin (first-generation), INK128 (second-generation), and RMC-6272 (third-generation) using in vitro dose–response testing, cell-cycle analysis, and immunoblotting. Furthermore, the efficacy of RMC-6272 was assessed in *NF2*-null 3D-spheroid meningioma models, and its in vivo potential was evaluated in 2 orthotopic meningioma mouse models.

Results. Treatment of meningioma cells revealed that, unlike rapamycin, RMC-6272 demonstrated superior growth inhibitory effects, cell-cycle arrest, and complete inhibition of phosphorylated 4E-BP1 (mTORC1 readout). Moreover, RMC-6272 had a longer retention time than INK128 and inhibited the expression of several eIF4E-sensitive targets on the protein level. RMC-6272 treatment of NF2 spheroids showed significant shrinkage in size as well as reduced proliferation. Furthermore, in vivo studies in mice revealed effective blockage of meningioma growth by RMC-6272, compared with vehicle controls.

Conclusions. Our study in preclinical models of NF2 supports possible future clinical evaluation of third-generation, investigational mTORC1 inhibitors, such as RMC-5552, as a potential treatment strategy for NF2.

Key Points

- Third-generation mechanistic target of rapamycin complex 1 (mTORC1) inhibitor RMC-6272 potently inhibits meningioma cell growth.
- RMC-6272 durably inhibits the mTORC1–4E-BP1 axis and reduces global translation.
- In NF2 meningioma models, RMC-6272 reduces size of 3D spheroids and mouse tumors.

Graphical Abstract

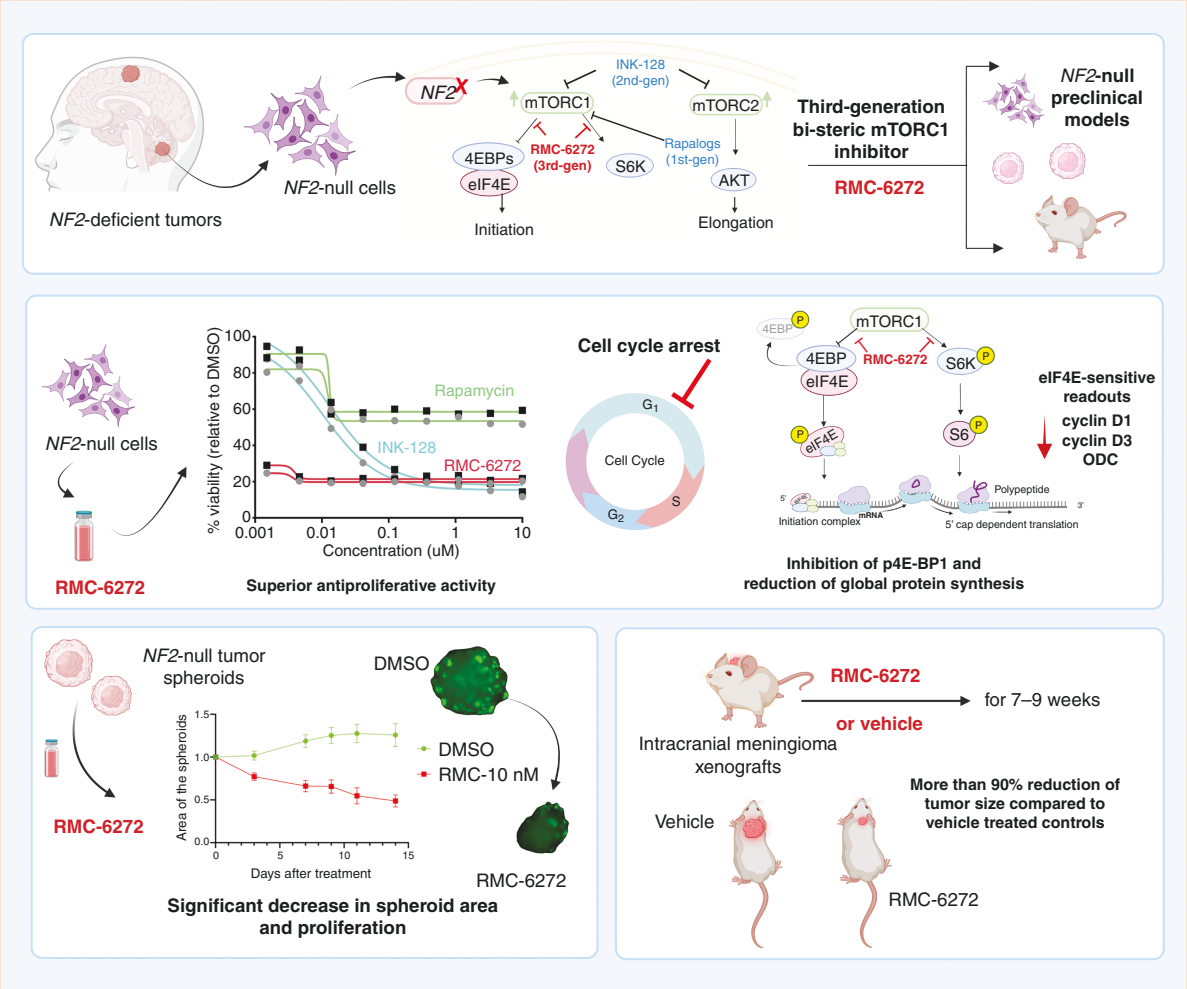

Importance of the Study

NF2-associated meningiomas are often progressive and are resistant to traditional chemotherapies highlighting the need for improved treatment strategies. Here, we evaluated the potential of third-generation, bi-steric mechanistic target of rapamycin complex 1 (mTORC1)-selective inhibitors, using the preclinical tool compound RMC-6272 in NF2 in vitro and in vivo models. Treatment of meningioma cell lines with RMC-6272 exhibited superior growth inhibitory effects and cell-cycle arrest, along with complete and durable inhibition of the mTORC1 pathway readout p4E-BP1. Furthermore, RMC-6272 inhibited global protein synthesis and decreased translation of several eIF4E-sensitive readouts. Additionally, RMC-6272 treatment significantly impeded the growth of *NF2*-deficient meningioma 3D spheroids and meningioma xenografts. Our results observed in 2D, 3D, and in vivo preclinical models of NF2 support future clinical evaluation of third-generation mTOR inhibitors as a potential treatment strategy for NF2.

NF2-related schwannomatosis (formerly neurofibromatosis type 2), hereafter referred to as "NF2," is caused by bi-allelic inactivating mutations in the *NF2* gene, encoding the tumor suppressor protein merlin.[1] NF2 is characterized by multiple nervous system tumors, including hallmark bilateral vestibular schwannomas and meningiomas observed in 80% of patients.[2,3] In addition, ~50% of sporadic meningiomas, the most common intracranial tumor in adults, show loss of *NF2*/merlin.[4] Meningiomas are resistant to standard chemotherapies; the current standard of care is surgery, and radiation can be used for inoperable, progressive, and higher grade meningiomas.

NF2-associated meningiomas often display higher grade, poor clinical outcome, and recurrence despite surgery.[5–7] Therefore, effective noninvasive therapies are urgently needed for both NF2-associated and sporadic tumors.

We previously established that loss of *NF2*/merlin leads to aberrant activation of mechanistic target of rapamycin complex 1 (mTORC1) signaling in *NF2*-deficient meningiomas and schwannomas.[8,9] Our findings led to NF2 clinical trials with everolimus, a rapalog, and first-generation, allosteric mTORC1 inhibitor, which demonstrated delayed tumor growth.[10–12] Among its many vital functions, mTORC1 signaling plays a fundamental role in regulating protein synthesis, primarily through phosphorylation of 2 key downstream substrates p70 ribosomal protein S6 kinase (S6K) and eIF4E-binding protein 1 (4E-BP1). The modest clinical response to rapalogs in NF2 patients may be attributed to incomplete inhibition of mTORC1, with effective attenuation of the mTORC1–S6K–S6 axis but only limited or no inhibition of the mTORC1–4E-BP1–eIF4E axis, which controls the rate-limiting step of 5′cap-dependent translation initiation.[13,14]

We also observed constitutive activation of the mTORC2–SGK1–NDRG1 signaling axis in *NF2*-deficient meningioma and Schwann cells (SCs)[15,16] for which treatment of NF2 preclinical models with second-generation, orthosteric mTOR kinase inhibitors (active site kinase inhibitors) AZD2014/vistusertib or INK128/TAK-228/sapanisertib reduced proliferation/growth more effectively than the first-generation mTORC1 inhibitor rapamycin.[15] This work led to a recently completed phase II single-arm clinical trial with vistusertib for NF2-associated meningiomas, which demonstrated high rates of stable disease for progressive meningiomas; however, this drug was poorly tolerated leading to premature withdrawal by many participants.[2] The significant toxicity of second-generation inhibitors like vistusertib may be attributed to the targeting of mTORC2, which regulates several crucial functions, such as glucose homeostasis and lipid metabolism.[17,18] While these findings indicate the importance of the mTOR pathway in NF2-associated tumors, they also highlight the need for improved mTORC1-specific compounds.

To address the limitations of first- and second-generation mTOR inhibitors, third-generation, "bi-steric" mTOR inhibitors were developed, exemplified by Rapalink-1.[14,19] This compound combined the specificity of the FKBP12-rapamycin binding domain from the first-generation rapamycin with the kinase inhibition property of the second-generation INK128, exhibiting a moderate 3- to 4-fold selectivity toward mTORC1 over mTORC2. Subsequently, improved bi-steric versions demonstrate increased selectivity by several-fold for mTORC1 over mTORC2, and have garnered recent attention for the treatment of several solid tumors, owing to their unique chemistry.[18,20–22] One such compound of this class is the investigational agent RMC-5552 which has over 30-fold selectivity for mTORC1 and is currently under clinical evaluation (https://clinicaltrials.gov/: NCT04774952 and NCT05557292). Based on the established importance of mTORC1 signaling in *NF2*-deficient meningiomas, we have explored the potential of RMC-6272, a preclinical tool compound representative of the clinical investigational agent RMC-5552.[20] Employing *NF2*-deficient immortalized and primary meningioma cell lines, we have demonstrated superior anti-proliferative activity of RMC-6272 in comparison to first- or second-generation mTOR inhibitors. More importantly, RMC-6272 robustly and durably inhibited phosphorylation of rapamycin-resistant substrate 4E-BP1 in *NF2*-deficient lines and decreased global translation as well as several eIF4E-sensitive readouts. Furthermore, we have generated clinically relevant *NF2*-null 3D-spheroid meningioma models (grade I and grade III) and validated the superior potency of the bi-steric compound in comparison with rapamycin or INK128. We also observed inhibitory effects of RMC-6272 by dose–response testing in CRISPR-modified *NF2*-null SCs and a 3D-spheroid schwannoma model generated from *NF2*-null SCs. Finally, RMC-6272 effectively blocked tumor growth in both NF2-associated and sporadic, *NF2*-deficient meningioma models.

Materials and Methods

See Supplementary Methods for additional details regarding cell lines, immunoblotting, lentiviral transduction, cell-cycle analysis, and immunofluorescence staining.

Cell Lines and Reagents

NF2-deficient meningioma lines included 4 immortalized lines, Ben-Men-1,[23] AG-NF2-Men derived from an NF2 patient WHO grade-I meningioma (L.-S.C., unpublished manuscript), MN1-LF,[24] and spontaneously immortalized KT21-MG1,[25,26] as well as 4 primary lines MN597 (grade II), MN646C (grade I), MN647C (grade I, with atypical features), and MN663 (grade II). Surgical collection of tumors was performed following Massachusetts General Hospital and Nationwide Children's Hospital IRB-approved Human Subjects protocols with informed consent. The genome-edited *NF2*-null Schwann cell line (clone S3) has been previously described.[27] Inhibitors included rapamycin from EMD Millipore, INK128/TAK-228 from Selleck Chemicals, and RMC-6272, generously provided by Revolution Medicines, Inc. Antibodies for phosphorylated S6 (pS6; S240/244), pS6 (S235/236), S6, pS6K (T389), S6K, p4E-BP1 (S37/46), p4E-BP1 (S65), 4E-BP1, pAkt (T308), pAkt (S473), Akt, p-mTOR (S2448), mTOR, ornithine decarboxylase (ODC), cyclin D1, cyclin D3, AlexaFluor 488-conjugate Ki-67 (D3B5), and PARP (detecting uncleaved and cleaved), as well as control Jurkat extracts (untreated or etoposide-treated) were from Cell Signaling Technologies. Other antibodies included β-actin from Santa Cruz Biotechnology and GAPDH from EMD Millipore, along with an anti-NF2/merlin polyclonal antibody that has been previously described.[28]

Dose–Response Testing

For meningioma lines Ben-Men-1, MN1-LF, MN646C, and MN663A, dose–response testing was performed in a 384-well format using the CellTiter-Glo cell viability kit (Promega) as previously described.[15] Briefly, ~20 hours post-seeding, cells were treated with serial dilutions of rapamycin, INK128, or RMC-6272 in full growth medium

and incubated for 72 hours (see figure legends for dosage point details). Relative luminescence units were measured using an EnVision 2103 Multilabel Reader (Perkin Elmer). Dose–response curves (DRCs) were plotted using GraphPad Prism 10 software, and the drug concentrations inhibiting cell growth by 50% (IC50) relative to DMSO were determined using nonlinear regression (curve fit) analysis. For AG-NF2-Men, cells were seeded in 96-well plates (Sarstedt), and the next day cells were treated with RMC-6272, INK128, or everolimus (see figure legend for dosage point details). Cell viability was assessed after 3 days by adding resazurin (Sigma) and measuring metabolic conversion to fluorescent resorufin (excitation 544 nm and emission 590 nm) on a SpectraMax M2e plate reader (Molecular Devices) as previously described.[29]

Global Protein Synthesis

Ben-Men-1, MN1-LF, and KT21-MG1 cells were incubated in the presence of RMC-6272 or vehicle for 1 hour in methionine and cysteine-free medium supplemented with 10% dialyzed serum, followed by the addition of 3 µL of EasyTag™ EXPRESS^{35}S Protein Labeling Mix (150–225 µCi/mL; Perkin Elmer Life Sciences) during the last 15 minutes of incubation. Then, cells were washed once with 1× PBS and directly lysed in 40 µL of RIPA buffer (50 mM Tris-HCl at pH 7.5, 150 mM NaCl, 1.0% NP-40, 0.5% sodium deoxycholate, and 0.1% SDS). Twenty microliters of the lysate was spotted onto Whatman 3 MM paper preblocked with 50× amino acids mix (ThermoFisher), dried, and placed in cold 10% trichloroacetic acid (TCA) for 20 minutes. Filters were then transferred to 5% TCA, boiled for 15 minutes, washed once with 5% TCA, once more with 95% ethanol, and dried. Radioactivity was determined by scintillation counting. The obtained counts were normalized to protein concentration in each sample, which had been determined by DC Protein Assay (Bio-Rad).

3D-Spheroid Model Generation and Inhibitor Treatment

Spheroids were generated using a well-established scaffold-free, liquid-overlay technique.[30–32] Briefly, 96-well plates were precoated with 1.5% (w/v) agarose. Following initial experiments to determine optimal cell numbers for successful formation of cell aggregates, single-cell suspensions of MN1-LF (3500 cells/well), KT21-MG1 (3000 cells/well), or *NF2*-CRISPR SCs (5000 cells/well) were seeded, followed by centrifugation at 1000 × *g* for 10 minutes. Cell aggregates were then incubated at 37°C, and spheroid growth was monitored daily. Once a diameter of ~200 µm was attained, treatment of MN1-LF and KT21-MG1 spheroids was initiated with rapamycin, INK128, or RMC-6272 at 10 nM, 100 nM, and 1 µM for each drug, respectively, with twice weekly treatment up to 14 days. For *NF2*-CRISPR SCs, treatment was initiated using 10 nM RMC-6272. Growth and shrinkage of spheroids over the course of treatment were assessed by unbiased region-of-interest analysis of area for individual spheroids using Adobe Photoshop 2023. All brightfield images were captured using a Nikon Eclipse TE2000-U microscope and NIS-Element AR 3.2 imaging software. Each experiment was performed in 3 biological replicates, with a minimum of $n = 4$ spheroids/treatment condition for each replicate. Spheroid area was plotted using GraphPad Prism10.

Quantifiable Skull-Base Meningioma Mouse Models

All animal experiments were performed according to the protocol approved by the Institutional Animal Care and Use Committee at Nationwide Children's Hospital. The skull-base meningioma models were generated as previously described.[26] Briefly, luciferase-expressing AG-NF2-Men-Luc2 cells (1×10^6 cells per mouse) were injected into the skull base of 8- to 12-week-old NSG (*NOD.Cg-Prkdc^{scid} Il2rg^{tm1Wjl}/SzJ*) mice (The Jackson Laboratory). Injected mice were subjected to weekly bioluminescence imaging (BLI) using an IVIS Spectrum In Vivo Imaging System (Perkin Elmer). Mice with successful tumor establishment, as defined by an increase in BL signal over at least 2 time points, were randomized into 3 groups and treated with RMC-6272 at 8 mg/kg ($n = 10$) or 3 mg/kg ($n = 5$), or vehicle (5% transcutol, 5% solutol HS15, and 90% water [v/w/v])[20] once a week by intraperitoneal (IP) injection. The effects of treatment on tumor growth were assessed by weekly BLI. The luminescence detected in each mouse was normalized to its pretreatment signal, and the mean and standard deviation of normalized luminescence for each treatment group were calculated and graphed. Similarly, luciferase-expressing Ben-Men-1-LucB cells[26] were injected to establish intracranial xenografts. Mice bearing established tumors were treated with 8 mg/kg of RMC-6272 or vehicle ($n = 7$/group) and imaged every week as described above. Statistical significance was determined using the longitudinal analysis module of the TumGrowth web tool,[33] https://kroemerlab.shinyapps.io/TumGrowth/, with linear mixed model fitting of normalized tumor volumes.

Results

Treatment of *NF2*-Null Meningioma Cell Lines With the Third-Generation mTOR Inhibitor RMC-6272 Potently Reduces Proliferation

With the recent development of bi-steric mTORC1-selective inhibitors, such as RMC-6272, we first sought to directly compare all 3 classes of mTOR inhibitors in cell viability assays. Initial dose–response testing was carried out in immortalized *NF2*-null meningioma lines Ben-Men-1 and MN1-LF using 9 dosage points for each compound in a standard range of 1.5 nM–10 µM (1:3 dilution series) treated for 72 hours. In agreement with our previous reports, DRCs for rapamycin showed minimal decrease in percent viability with IC50 (defined as drug concentration showing 50% inhibition relative to DMSO) unable to be calculated since the maximum response (MR) at the highest dose of 10 µM showed <50% inhibition. DRCs for INK128 treatment showed increased activity with IC50s of 15.3 nM (MR = 88% inhibition) and 22.6 nM (MR = 86% inhibition) in Ben-Men-1 and MN1-LF, respectively.

In contrast, RMC-6272 treatment showed an extreme level of potency with IC50 being undetermined since both cell lines showed >70% inhibition even at the lowest dose (1.5 nM; Figure 1A). Due to the high potency of RMC-6272, we next performed 9-point testing as above, lowering the concentration range by 10-fold (152 pM–1 μM), and extended testing to include 2 primary meningioma lines in addition to Ben-Men-1 and MN1-LF. Again, for all 4 lines,

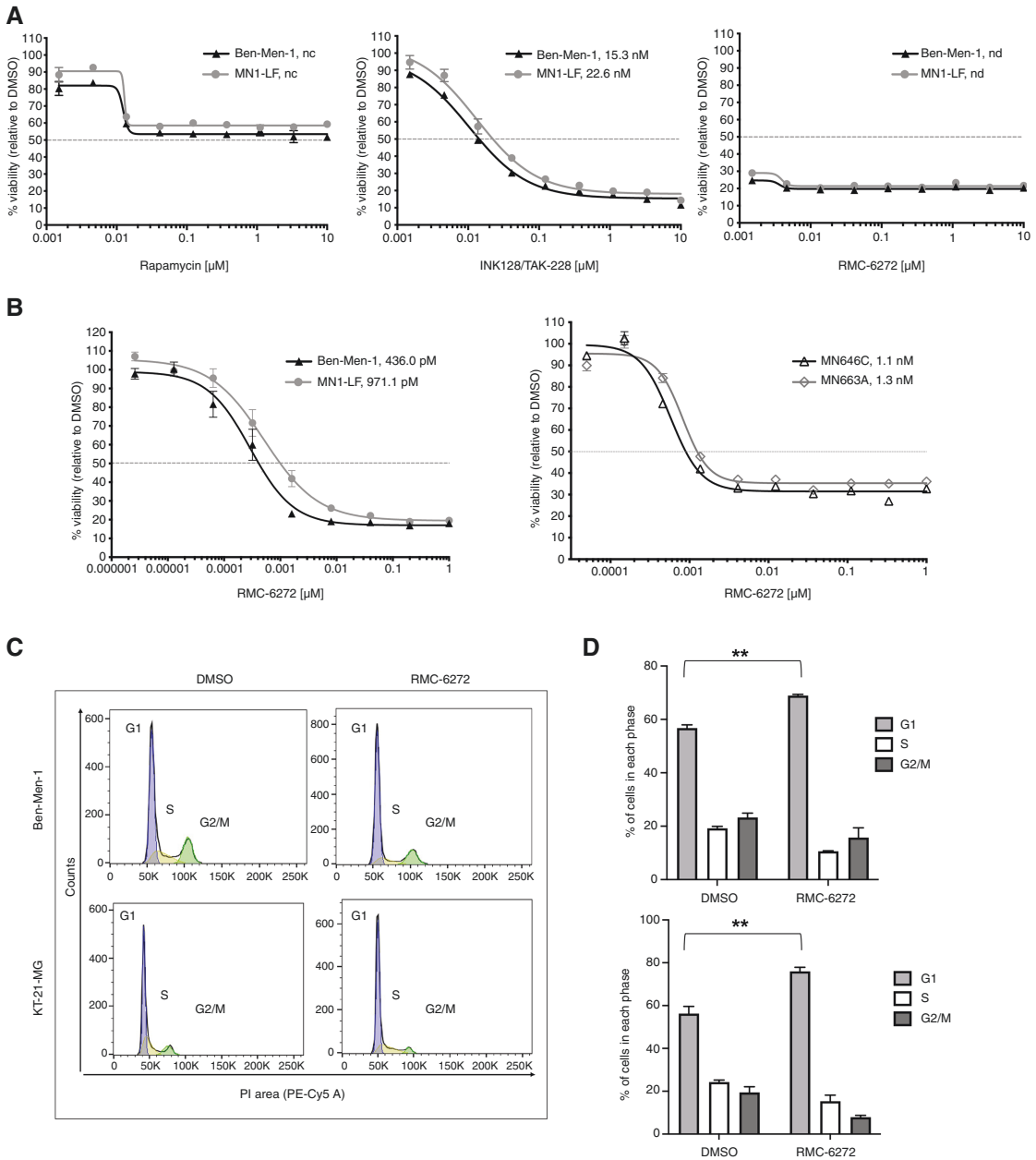

Figure 1. RMC-6272 treatment leads to reduced cell viability and induces cell-cycle arrest in *NF2*-null meningioma cell lines. (A) Dose–response curves (DRCs) are shown representing percent cell viability relative to DMSO for human *NF2*-null immortalized meningioma lines Ben-Men-1 and MN1-LF. Comparison of mTOR inhibitors including rapamycin (first-generation, left plot), INK128 (second-generation, middle plot), and RMC-6272 (third-generation, right plot) in cell lines treated with 9 dosage points (1.5 nM–10 μM, 1:3 serial dilution) for each drug demonstrates high potency of RMC-6272. Data represents a single experiment, performed in triplicate, ± SEM. (B) Due to high potency (shown in A), dose–response testing was repeated for RMC-6272 with 9 dosage points (2.6 pM–1 μM, 1:5 serial dilution) in Ben-Men-1 and MN1-LF (left plot), as well as 10 dosage points (51 pM–1 μM, 1:3 serial dilution) in *NF2*-null primary lines MN646C and MN663A (right plot). Data represents 3 independent experiments (4 replicates/experiment), ± SEM. IC50s for respective cell lines (A and B) were determined using GraphPad Prism10 (shown in the upper right legend for each graph). nc, unable to be calculated; nd, undetermined. (C and D) Cell-cycle data for Ben-Men-1 ($n = 3$) and KT21-MG ($n = 3$) treated with 10 nM RMC-6272 for 24 hours is shown (C as a representative). Quantitation of cell-cycle data (D) represents the percentage of cells in each phase of the cell cycle where each data point denotes average of 3 biological replicates, ± SEM. Cell-cycle analysis revealed that RMC-6272 treatment leads to a significant G1 arrest in both the cell lines compared with DMSO controls. $^{*}P < .05$, $^{**}P < .01$, calculated by one-tailed Student's *t* test.

potent inhibition was found even at the lowest dose of 152 pM, with primary meningioma lines showing slightly decreased sensitivity (data not shown). Therefore, to determine the IC50 for RMC-6272, we next carried out testing for Ben-Men-1 and MN1-LF using 9 dose points of 2.6 pM–1 μM (1:5 dilution series) that demonstrated IC50s of 436.0 pM (MR = 82% inhibition) and 971.1 pM (MR = 80% inhibition), respectively. For *NF2*-null primary meningioma lines MN646C and MN663A, 10 dose points of 51 pM–1 μM (1:3 dilution series) showed IC50s of 1.1 nM (MR = 67% inhibition) and 1.3 nM (MR = 64% inhibition), respectively (Figure 1B).

Given our results showing potent growth inhibition in RMC-6272-treated cells, we next tested the effect of RMC-6272 on cell cycle. We performed flow cytometry analysis of propidium iodide-stained Ben-Men-1 and observed a significant G1 phase arrest compared with the DMSO control. We also tested the malignant meningioma line KT21-MG1 and observed similar results (Figure 1C). Furthermore, we assessed the induction of apoptosis by RMC-6272 in Ben-Men-1 and MN1-LF cells and observed no PARP cleavage, denoting that RMC-6272 treatment does not lead to apoptosis in meningioma cells (Supplementary Figure 1). These results demonstrate that RMC-6272 is superior to rapamycin and INK128 to inhibit cell growth and leads to a significant G1 arrest in meningioma cell lines.

RMC-6272 Effectively Inhibits Both Axes of mTORC1 Signaling in NF2-Null Meningioma Cell Lines

We next examined the effect of RMC-6272 treatment on the phosphorylation status of key downstream mTORC1 pathway readouts (Figure 2A) by immunoblotting following 24-hour treatment with RMC-6272 compared with rapamycin or INK128. As expected, all 3 compounds efficiently inhibited the mTORC1–S6K–S6 axis, as evidenced by the inhibition of pS6K (T389) and its downstream target pS6 (S240/244) in immortalized and primary meningioma lines. Furthermore, treatment with either 10 nM RMC-6272 or 200 nM of INK128 demonstrated complete inhibition of p4E-BP1 (S65) as well as p4E-BP1 (T37/46), whereas 50 nM rapamycin had minimal effect on p4E-BP1 (Figure 2B and C). As expected, rapamycin did not inhibit phosphorylation of Akt (S473), the direct target of mTORC2, while INK128 potently blocked pAkt (S473), in all immortalized and primary meningioma lines tested. Importantly, 10 nM RMC-6272 treatment did not inhibit pAkt (S473) in MN1-LF, MN597, and MN663 cells (Figure 2B and C), demonstrating mTORC1-selectivity, consistent with the previous reports in other tumor types. However, in Ben-Men-1 cells, we detected inhibition of mTORC2 target pAkt (S473), suggesting possible heterogeneity in drug response (Figure 2B). We, therefore, decreased treatment doses to 200 pM, 1 nM, and 2 nM in Ben-Men-1 cells (representing approximately 0.5×, 2.5×, and 5× of IC50 concentration) and observed that the lowest dose (200 pM) of RMC-6272, robustly inhibited both S6K and 4E-BP1 arms of mTORC1 signaling while retaining mTORC1 selectivity as evident by no changes in the phosphorylation status of mTORC2 target pAkt (S473; Supplementary Figure 2). Taken together, these results indicate potent inhibition of mTORC1 pathway readouts by RMC-6272 in all the immortalized and primary meningioma cell lines along with mTORC1 specificity.

RMC-6272 Exhibits Durable Inhibition of mTORC1 Signaling

We next assessed the duration of action of RMC-6272 compared with second-generation INK128 in *NF2*-deficient meningioma lines since sustained target inhibition provides a potential opportunity for intermittent dosing in patients.[22,34] In time-course experiments, we compared RMC-6272 with INK128 to assess retention time, or the time it took to re-activate mTORC1 signaling following drug washout. MN1-LF and KT21-MG1 cells were treated for 24 hours with INK128 or RMC-6272 followed by cell lysis at 0, 3, 8, and 24 hours post-drug washout. Immunoblotting revealed sustained inhibition of mTORC1 readouts p4E-BP1 (T37/46 or S65), pS6K (T389), and pS6 (S240/244) for RMC-6272 through 24 hours of washout in MN1-LF cells (Figure 3 left panel). Immunoblots of KT21-MG1 cells also reflect a similar trend where RMC-6272 demonstrated sustained inhibition for all the mTORC1 readouts except pS6K, which was reactivated within 24 hours (Figure 3 right panel). In contrast, in cell lines treated with INK128, reactivation of p4E-BP1 and pS6K was observed within 3 hours of washout. Our results reveal durable blockage of mTORC1 signaling by RMC-6272, compared with a short retention time of 3 hours for INK128.

RMC-6272 Treatment Reduces Global Translation and Downregulates eIF4E-Sensitive Readouts

We previously reported that *NF2* loss in meningioma cells leads to constitutive activation of the mTORC1 pathway, including the mTORC1–S6K–S6 and the mTORC1–4E-BP1 downstream signaling axes.[9] When in an unphosphorylated state, 4E-BP1 functions as a translational repressor by binding and sequestering the eIF4E subunit from the heterotrimeric eIF4F complex. Upon activation, mTORC1 directly phosphorylates 4E-BP1 leading to its dissociation from eIF4E, allowing eIF4F assembly and initiation of 5′ cap-dependent mRNA translation. Given that RMC-6272, unlike rapamycin, efficiently blocked the mTORC1–4E-BP1 axis in our meningioma cells, we next performed protein labeling assays to compare the effects of rapamycin vs RMC-6272 on global translation in Ben-Men-1, MN1-LF, and KT21-MG1 cell lines. Treatment for 1 hour with 10 nM RMC-6272 led to a much greater reduction in 35S incorporation when compared to 50 nM rapamycin treatments where minimal changes were observed (Figure 4A).

Furthermore, mRNAs showing long, G/C-rich 5′-UTRs with stable secondary structure are considered as "weak mRNAs" and have been reported to be strictly dependent on eIF4E for their translation, including ornithine decarboxylase (ODC), cyclins D1 and D3, B-cell lymphoma 2 (BCL2) and MYC.[35,36] We next examined the protein levels of some eIF4E-sensitive targets by immunoblotting in Ben-Men-1, MN1-LF, and KT21-MG1 and observed a more pronounced

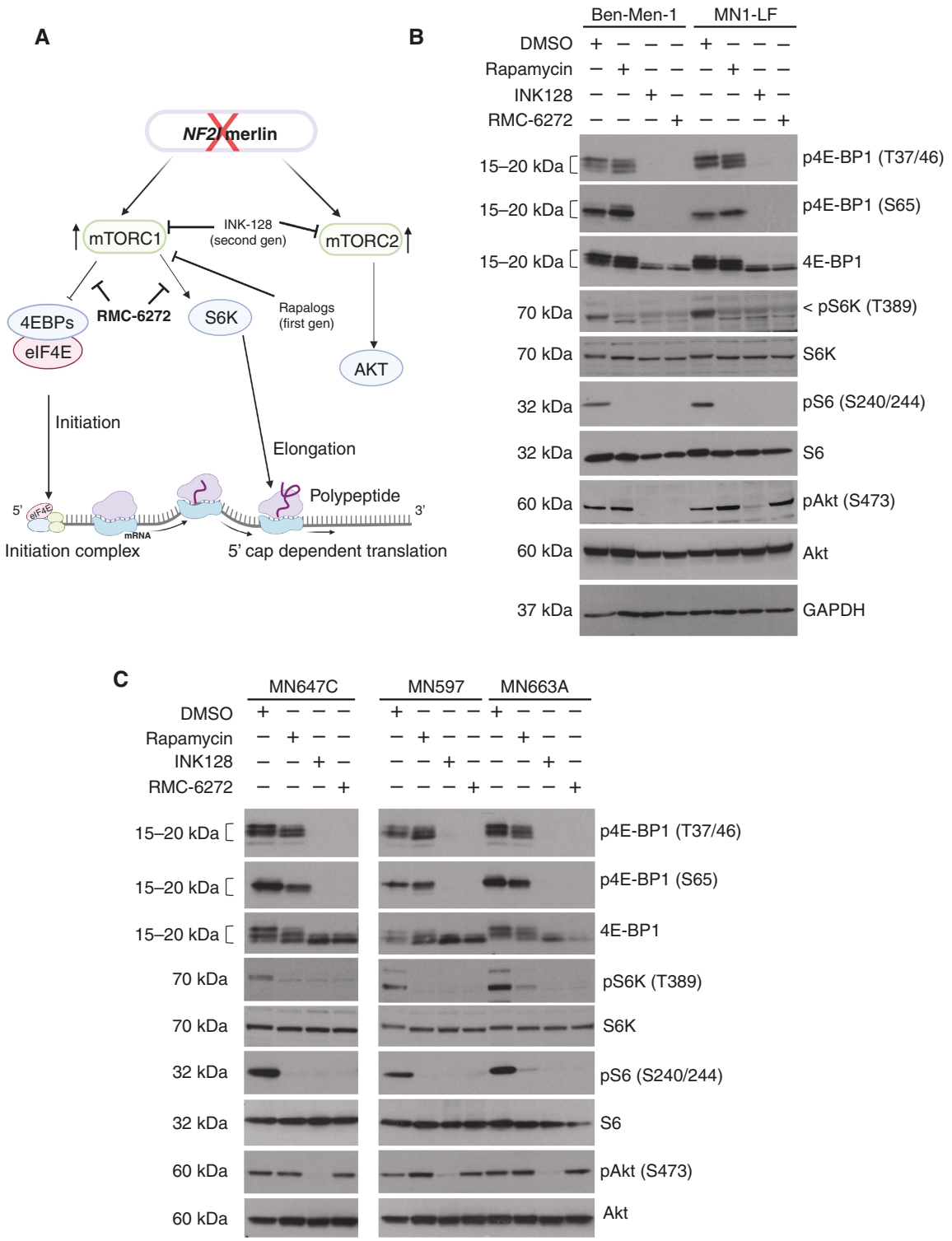

Figure 2. Treatment with RMC-6272 potently and selectively inhibits mTORC1 signaling in *NF2*-null cells. (A) Schematic representation of mTOR pathway regulation upon *NF2* loss showing 2 downstream signaling axes of mTORC1 (4E-BP1–eIF4E and pS6K–S6), as well as the mTORC2–Akt pathway, along with 3 generations of mTOR inhibitors. (B and C) Immunoblotting of *NF2*-null meningioma lines, including immortalized Ben-Men-1 and MN1-LF (B) as well as primary MN647D, MN597, and MN663 (C), treated for 24 hours with rapamycin (50 nM) revealed inhibition of pS6K (T389; mTORC1–S6K axis) with no attenuation of p4E-BP1 (T37/46 or S65; mTORC1–4E-BP1 axis). In contrast, treatment with INK128 (200 nM) or RMC-6272 (10 nM) inhibited both mTORC1 axes, while only INK128 blocked pAkt (S473; mTORC2 readout). Respective total protein readouts and GAPDH served as controls. A representative immunoblot has been shown from $n = 3$ independent experiments for the immortalized lines and $n = 1$ for primary cell lines.

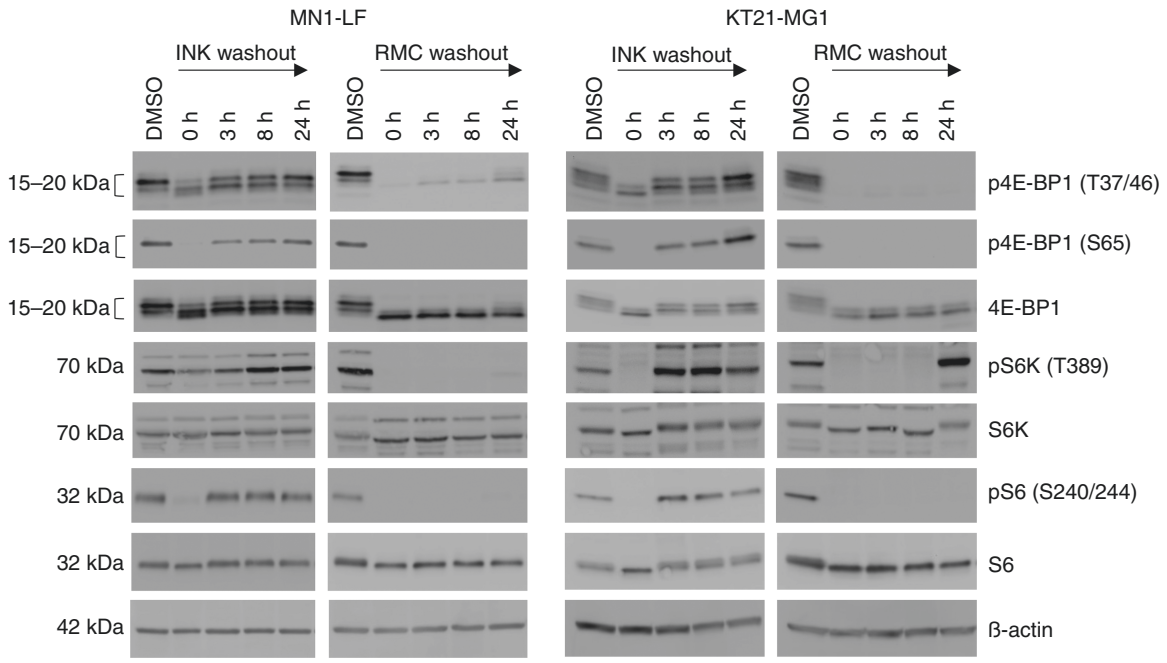

Figure 3. Treatment with RMC-6272 leads to sustained inhibition of mTORC1 targets in *NF2*-null meningioma cells. Immunoblotting was carried out for immortalized MN1-LF (left panel) and KT21-MG1 (right panel) meningioma lines treated with 200 nM INK128 (INK) or 10 nM RMC-6272 (RMC) for 24 hours followed by exchange for fresh growth medium without drugs to initiate washout. Lysates were collected to assess time to mTORC1 pathway reactivation after drug washout at indicated time points. Reactivation of mTORC1-specific readouts p4E-BP1 T37/46, p4E-BP1 S65, pS6K T389, and pS6 S240/244 was observed within 3 hours of INK128 removal. In contrast, RMC-6272 treated cells demonstrated sustained inhibition through 24 hours after drug removal, with the exception of pS6K T389 that showed reactivation in KT21-MG1 cells at 24 hours after drug removal. Representative immunoblot blots are shown from at least $n = 2$ independent experiments. β-actin serves as a loading control.

decrease in ODC, cyclin D1, and cyclin D3 upon RMC-6272 treatment, with rapamycin showing more modest changes (Figure 4B) and no change observed in BCL2 or MYC (data not shown). These data suggest that the decrease in some eIF4E-sensitive targets may be due to more efficient inhibition of phosphorylated 4E-BP1 by RMC-6272. To test this, we next employed RNA interference in Ben-Men-1 cells transduced with 2 independent short hairpin RNAs (shRNAs) targeting 4E-BP1. Immunoblotting confirmed suppression of 4E-BP1 along with increased levels of cyclin D1, cyclin D3, and ODC (Figure 4C). These data suggest that the mTORC1–4E-BP1–eIF4E axis plays an important role in increased translation upon *NF2* loss, and third-generation mTORC1 inhibitors such as RMC-6272 are potentially superior in suppressing translation in *NF2*-deficient meningioma cells.

Establishment of 3D In Vitro Models of NF2 and Evaluation of RMC-6272 for Therapeutic Potential

Three-dimensional (3D) multicellular tumor spheroids (MCTS) are gaining increased recognition for preclinical drug testing since they more closely resemble the morphological and functional properties of an in vivo tumor when compared with traditional 2D culture systems.[37–40] For example, 3D spheroids develop an inner necrotic core enclosed by a hypoxic area followed by a proliferating zone simulating the microenvironment of a vascular tumor and conferring a higher degree of biological relevance.[41] Here we sought to generate 3D MCTS for NF2 and evaluate the therapeutic efficacy of RMC-6272 in this model. To generate 3D spheroids from *NF2*-deficient lines MN1-LF (grade I with atypical features) and KT21-MG1 (grade III malignant), we utilized a simple and reproducible scaffold-free method of forced floatation to obtain single spheroids in a 96-well format. Among many factors, optimal cell number contributes to the successful formation of uniform homogenous spheroids. Following optimization, we utilized 2500 and 3000 cells/well for MN1-LF and KT21-MG1, respectively. Based on previously described methods, spheroid growth was monitored daily where cells followed a predicted pattern of formation including (i) aggregation within 24 hours of seeding, (ii) aggregate compaction into a cohesive spheroid structure due to secretion of extracellular matrix over 3–5 days, followed by, and (iii) spheroid growth to a minimal diameter of ~200–250 μm prior to initiating drug treatment.[42] Spheroids were subsequently treated with increasing doses (10 nM, 100 nM, and 1 μM) of rapamycin, INK128 and RMC-6272 for 2 weeks. Consistent with results observed in 2D meningioma cultures, rapamycin had minimal effect on spheroid size for all doses tested, whereas INK128 treatment revealed a dose-dependent reduction in size after 14 days of treatment for both MN1-LF and KT21-MG1 spheroids (Figure 5; Supplementary Table 1). Interestingly, for both

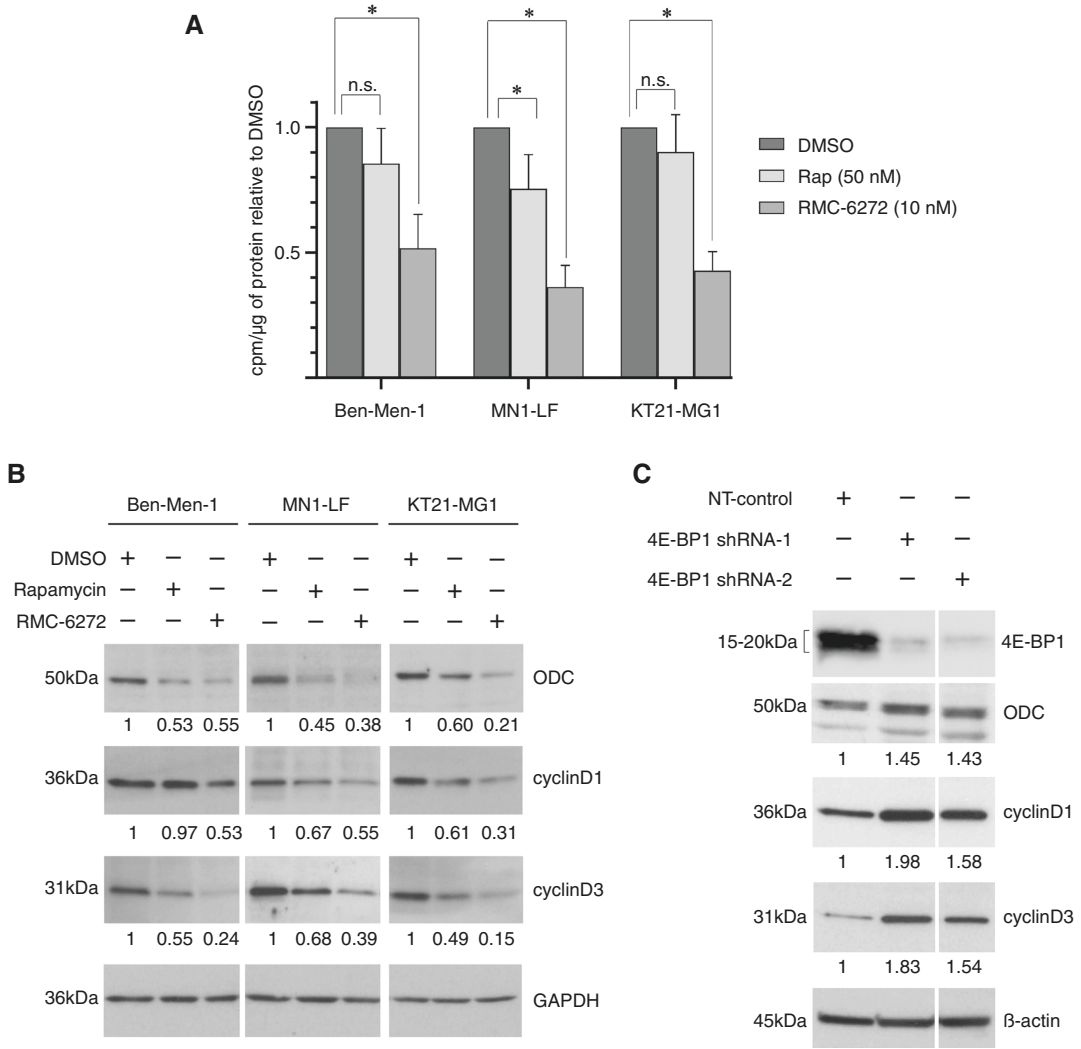

Figure 4. RMC-6272 treatment reduces protein synthesis and downregulates eIF4E-sensitive translational targets. (A) Protein metabolic labeling of *NF2*-null meningioma cell lines revealed a significant reduction in global protein synthesis upon treatment with 10 nM RMC-6272 compared with 50 nM rapamycin treatment. Data represents counts per minute (cpm)/µg of protein plotted using GraphPad Prism10, relative to DMSO-treated controls (3 biological replicates performed in duplicate; n.s., nonsignificant; $*P < .05$). (B) Immunoblot analysis of eIF4E translational readouts ODC, cyclin D1, and cyclin D3 in *NF2*-null meningioma lines showed a greater reduction with all 3 lines treated for 24 hours with RMC-6272 (10 nM), compared with rapamycin (50 nM, 24 hours) showing a more modest reduction ($n = 3$). A representative immunoblot along with quantitation by ImageJ/Fiji is shown for each readout protein relative to GAPDH. (C) Immunoblotting of Ben-Men-1 cells transduced lentivirus with 2 independent shRNAs targeted human 4E-BP1 revealed increased levels of eIF4E-sensitive readouts ODC, cyclinD1, and cyclin D3 compared with non-targeting (NT) shRNA control. Quantitation by ImageJ/Fiji is shown for each readout protein relative to housekeeping controls (GAPDH or β-actin).

the grade I and grade III spheroids, treatment with the lowest dose of RMC-6272 (10 nM) led to >70% decrease in spheroid size after 14 days versus DMSO controls, while treatment with rapamycin or INK128 at the same dose led to only minimal reduction of ~20% in the same timeframe (Figure 5B and C). In addition, since development of vestibular schwannomas is a hallmark of NF2, we tested the efficacy of RMC-6272 in a CRISPR-modified, *NF2*-null human Schwann cell (SC) line. As with meningioma cells, dose–response testing in *NF2*-null SCs, using 9 dose points of 2.6 pM–1 µM (1:5 dilution series), demonstrated high potency for RMC-6272 with an IC50 of 33.5 pM (MR = 69.8% inhibition). We further assessed the effects of 10 nM RMC-6272 treatment on *NF2*-null SC spheroids and observed reduction in size versus DMSO control, similar to meningioma spheroids (Supplementary Figure 3). These data again highlight the improved therapeutic potential of third-generation mTOR inhibitors for NF2-related tumors.

To understand the inhibitory effect of RMC-6272 on spheroid size, we performed immunofluorescence (IF) staining for the proliferation marker Ki-67. Results demonstrate a global decrease in Ki-67 intensity upon RMC-6272 treatment compared with DMSO, indicating reduced proliferation in the treated spheroids (Figure 5D and E).

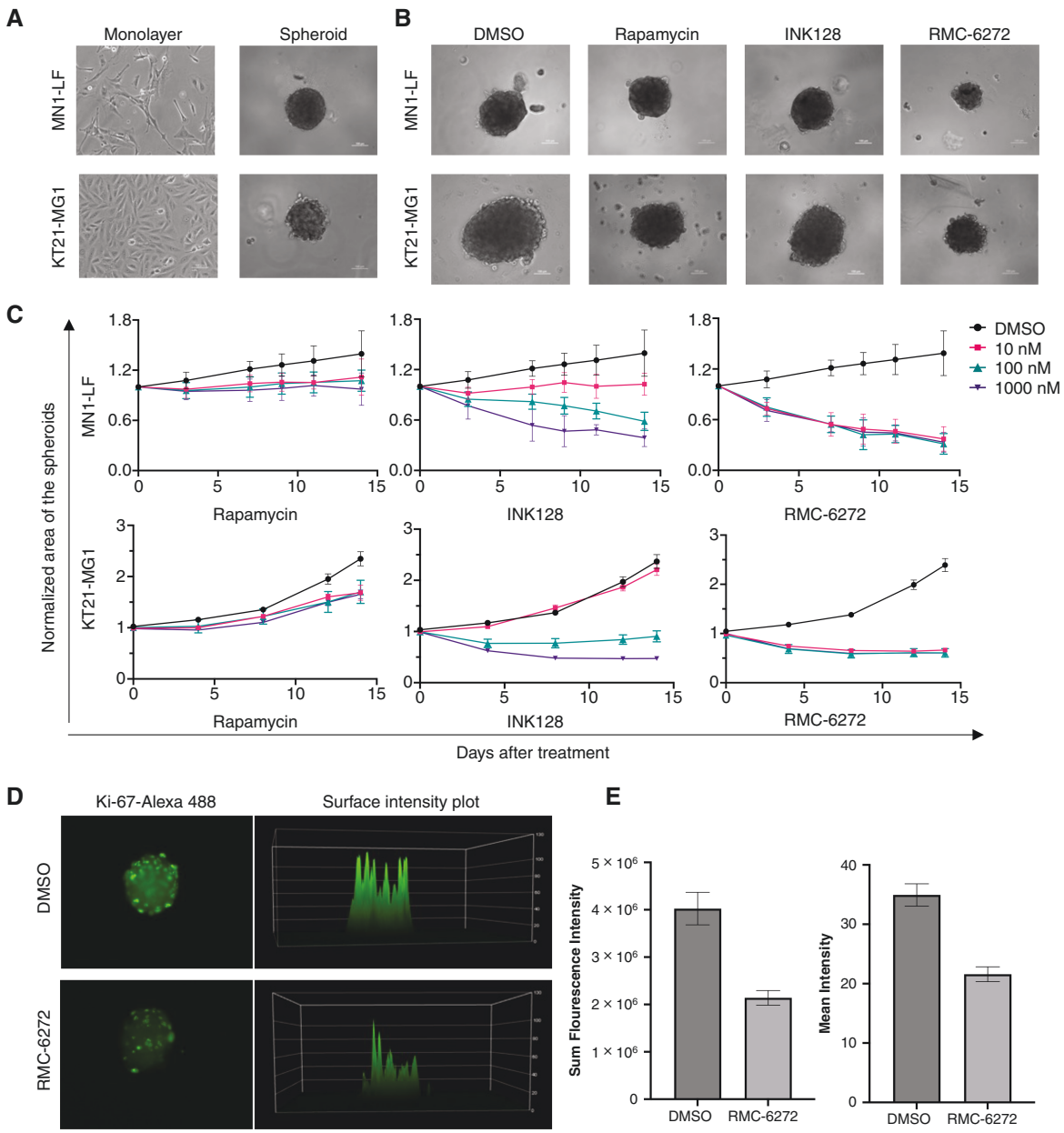

Figure 5. RMC-6272 treatment remains effective in 3D-spheroid models of NF2 meningioma and potently reduces the size of the spheroids. (A) Brightfield images of meningioma spheroids were generated from MN1-LF (grade I with atypical features) and from KT21-MG1 (grade III malignant) cells after day 7, alongside their respective monolayer images. (B) Representative brightfield images of MN1-LF and KT21-MG1 spheroids after 9-day treatment show a marked decrease in spheroid size with 10 nM RMC-6272 (third-generation) versus 10 nM of rapamycin or 10 nM INK128. (C) Quantitation of spheroid area is shown for MN1-LF and KT21-MG1 treated with 10 nM, 100 nM, and 1 μM of rapamycin, INK128, or RMC-6272, with superior effects observed for all doses of RMC-6272. Treatment was carried out twice a week for 14 days, and brightfield images were captured at indicated time points. Data was plotted using GraphPad Prism10 and represents mean area ± SEM from $n = 2$ independent experiments having a minimum of $n = 4$ spheroids per condition. (D) Representative fluorescent microscope images of MN1-LF spheroids demonstrating decreased Ki-67 expression as evident from the decreased fluorescence intensity in the RMC-6272 treated spheroids compared to DMSO-treated control along with surface intensity plot profile. (E) Average of sum fluorescence intensity and mean fluorescence intensity of $n = 6$ spheroids has been measured and plotted with GraphPad Prism10 along with ± SEM.

We next asked whether the reduction in spheroid size was attributed to cell death or apoptosis. Using a caspase 3/7 green detection reagent kit or propidium iodide staining, we found no significant induction of cell death or apoptosis (data not shown), suggesting that the observed reduction in the spheroid area might be due to decreases in cell proliferation as well as cell size, for which mTORC1 signaling is known to play a major role. Overall, our studies in 3D models of NF2 reveal superior efficacy of RMC-6272 and validate the results of the 2D platform,

thus providing a conducive basis to assess RMC-6272 in in vivo models of NF2.

RMC-6272 Effectively Blocks the Growth of Intracranial Meningioma Xenografts

To evaluate the antitumor activity of RMC-6272, we employed 2 quantifiable, orthotopic meningioma xenograft models established using luciferase-expressing AG-NF2-Men-Luc2 and Ben-Men-1-LucB cells. Like the Ben-Men-1 cell line, the AG-NF2-Men line was established from a grade I meningioma by telomerase immortalization; however, AG-NF2-Men cells were derived from an NF2 patient's tumor (L.-S.C., unpublished manuscript). The analysis of DRCs in AG-NF2-Men cells showed RMC-6272 to possess potent growth inhibitory activity with an IC50 value of ~250 pM for RMC-6272 (Supplementary Figure 4). Treatment of AG-NF2-Men cells with 200 pM, 1 nM, and 2 nM of RMC-6272 (representing approximately 1×, 5×, and 10× IC50) also efficiently inhibited pS6 and completely impaired 4E-BP1 phosphorylation even at 200 nM (~1× IC50). In addition, RMC-6272 retained mTORC1 selectivity in AG-NF2-Men cells as the pAkt (S473) levels were not affected by RMC-6272 treatment at 1× and 5× IC50 (Supplementary Figure 5).

Subsequently, we treated mice bearing actively growing, intracranial AG-NF2-Men-Luc2 tumors with 3 or 8 mg/kg of RMC-6272, or vehicle as the control. As reported previously,[20] both doses of RMC-6272 were well-tolerated and did not cause any overt weight loss in treated mice (data not shown). RMC-6272 at 3 mg/kg shrank AG-NF2-Men-Luc2 tumors by ~50% relative to their pretreatment sizes after 3 weeks of treatment (Figure 6A). However, tumor growth slowly started after the fourth treatment week. Overall, 3 mg/kg of RMC-6272 reduced tumor growth by ~94% after 9-week treatment, compared to vehicle-treated controls (Figure 6A and B). Interestingly, RMC-6272 at 8 mg/kg caused a greater tumor shrinkage to ~22% of the original tumors after 4-week treatment. While there was a small amount of tumor regrowth afterward, tumor shrinkage was still detectable after 10 weeks. To examine the possibility of retreatment, we stopped treating one cage of mice that had been treated with 8 mg/kg of RMC-6272 for 11 weeks and found that upon cessation of treatment, the tumors slowly regrew over the following 3 weeks (Figure 6C). However, when the treatment was reinitiated from weeks 14 to 18, tumor shrinkage was observed again.

Similarly, we treated mice bearing established Ben-Men-1-LucB xenografts with 8 mg/kg of RMC-6272 or vehicle. RMC-6272 treatment resulted in tumor shrinkage to ~60% of the original tumor sizes after 3 weeks (Figure 6D). Some tumor growth was observed from week 4, and the mean luminescence signal emitted by tumors treated with RMC-6272 for 8 weeks grew to about 2-fold of that of the original tumors. However, compared to vehicle controls, RMC-6272 suppressed tumor growth by ~99% after 7 weeks of treatment.

Together, both the in vitro and in vivo data suggest that RMC-6272 possesses potent antitumor activity in *NF2*-deficient sporadic and NF2-associated meningiomas.

Discussion

Our previous work demonstrating activation of mTOR signaling in *NF2*-deficient meningiomas and schwannomas led to clinical trials testing first- and second-generation mTOR inhibitors in NF2-related tumors. However, drawbacks have been observed for both classes of compounds. For first-generation allosteric rapalogs, tumor stabilization was observed with no shrinkage, possibly owing to inefficient blockage of the mTORC1 substrate 4E-BP1.[10–12] Whereas the second-generation orthosteric inhibitor vistusertib, while attenuating S6K and 4E-BP1 and showing more promising results, was poorly tolerated in patients,[2] potentially due to targeting of mTORC2, which regulates several crucial metabolic processes.[17,18] Here, we have tested the potency of a third-generation inhibitor RMC-6272, a tool compound representative of the clinical investigational agent RMC-5552, in *NF2*-deficient preclinical models. We observed superior inhibition of proliferation in both immortalized and primary meningioma lines upon RMC-6272 treatment, with IC50s in the picomolar range, compared to first- or second-generation mTOR inhibitors. We also noted significant cell-cycle arrest in immortalized grade I and grade III meningioma lines upon RMC-6272 treatment which is consistent with recent reports using bi-steric mTORC1 inhibitors for other tumor models.[34,43,44] However, we did not detect induction of apoptosis, which differs from recent studies in several cancer types including bladder, renal, and breast where RMC-6272 treatment induced apoptosis, supporting a cell/tumor context-dependent process in *NF2*-deficient meningiomas.[18,45] In addition, consistent with previous reports, we observed mTORC1 selectivity with effective inhibition of rapamycin-sensitive (S6K) and rapamycin-resistant (4E-BP1) substrates upon RMC-6272 treatment in primary and immortalized meningioma lines. It should be noted that in Ben-Men-1 cells, we initially detected inhibition of the mTORC2 substrate pAkt (S473) when treated with RMC-6272; however, upon lowering the treatment doses to the picomolar range, we observed mTORC1 selectivity in this cell line. Importantly, we found durable inhibition with a prolonged time to reactivation of mTORC1 signaling after washout of RMC-6272 versus INK128. It will be of interest to determine if this will be beneficial in a clinical setting as longer drug retention time provides the opportunity for reduced/intermittent dosing schedules.[22,34]

Given that 4E-BP1 functions as a major player to controlling 5′ cap-dependent translation,[35] we evaluated translation changes upon RMC-6272 treatment and observed a robust decrease in global protein synthesis in all meningioma lines tested in comparison with rapamycin. Furthermore, we observed a decrease in the translation of eIF4E-sensitive targets ODC, cyclin D1, and cyclin D3 protein levels. To gain further mechanistic insight, we performed shRNA of 4E-BP1 which confirmed increased levels of ODC, cyclin D1, and cyclin D3 substantiating the importance of inhibiting the mTORC1–4E-BP1–eIF4E axis. Interestingly, ODC is the first rate-limiting enzyme in the biosynthesis of polyamines which play a major role in

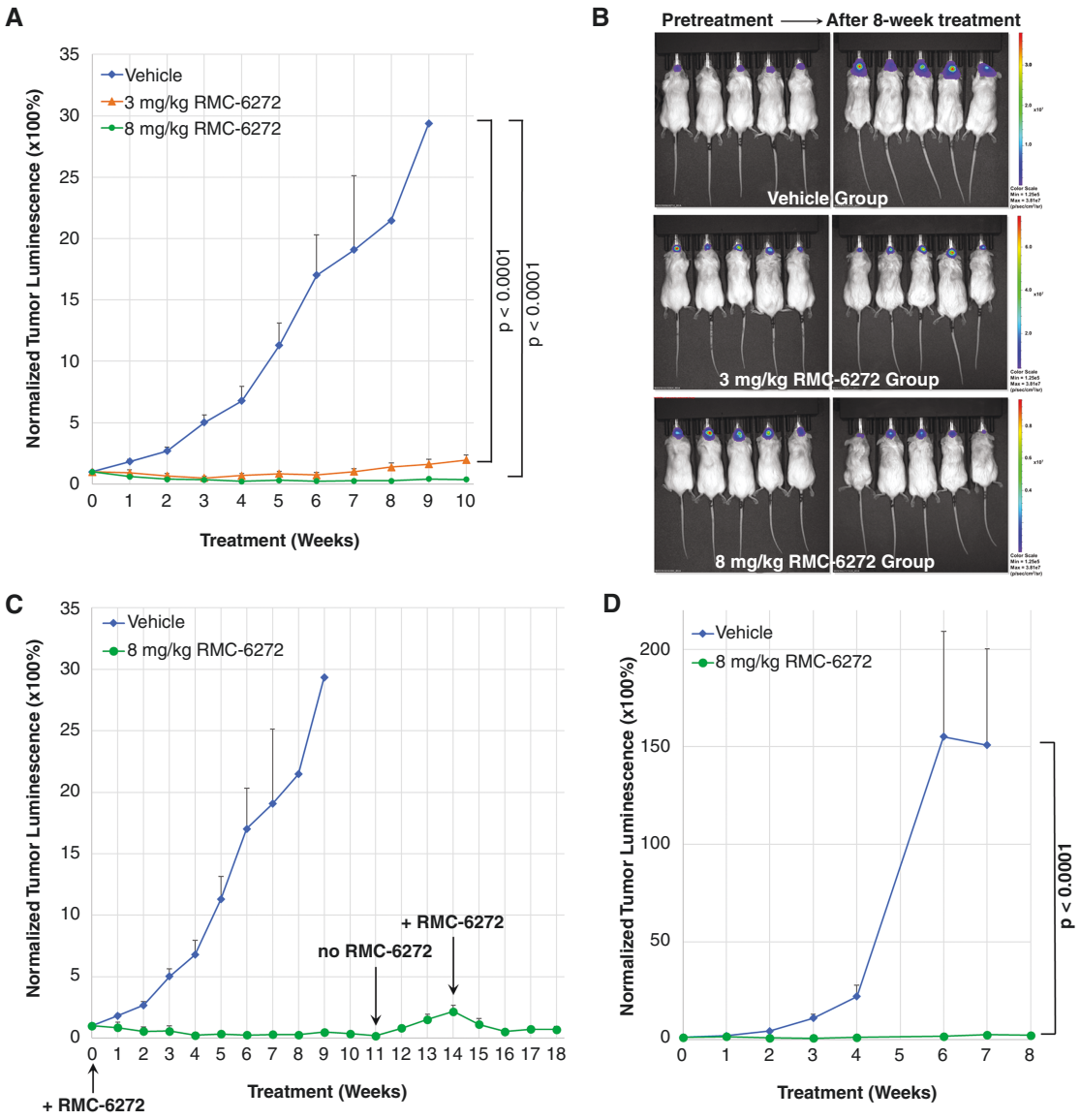

Figure 6. RMC-6272 effectively blocks the growth of intracranial AG-NF2-Men-Luc2 and Ben-Men-1-LucB meningioma xenografts. (A–D) NSG mice bearing actively growing AG-NF2-Men-Luc2 tumors were treated with 3 or 8 mg/kg of RMC-6272, or vehicle, and tumor growth was monitored by BLI. RMC-6272 at 3 mg/kg profoundly suppressed tumor growth by ~94% after 9 weeks of treatment, compared to vehicle controls, while the 8 mg/kg dose resulted in tumor shrinkage throughout the 10-week treatment (A). Representative bioluminescence images of groups of AG-NF2-Men-Luc2B meningioma-bearing mice at pretreatment or after 8 weeks of treatment with vehicle, or 3 or 8 mg/kg of RMC-6272 are shown (B). Upon cessation of treatment for a cohort of mice that had been treated with 8 mg/kg of RMC-6272, the tumors slowly regrew over the following 3 weeks, but tumors regressed again when the treatment was resumed (C). Similarly, NSG mice bearing established Ben-Men-1-LucB xenografts were treated with RMC-6272 at 8 mg/kg or vehicle, and the treatment effects were assessed by weekly BLI with the exception of the fifth-week time point due to inaccessibility of the IVIS Spectrum scanner. Potent tumor growth suppression was observed over the 8-week treatment period (D). Graphs show the means and standard errors of normalized tumor bioluminescence. The *P*-values were calculated from log-transformed normalized tumor volume using the cross-sectional functionality of the TumGrowth web tool ([33]; https://kroemerlab.shinyapps.io/TumGrowth/) using generalized least squares fit by maximum likelihood. The week 6 time point was chosen for both xenograft models as this was the last time point when the tumor BLI of at least 5 vehicle-treated control mice were measured.

cell growth and differentiation and induction of angiogenesis making it an attractive therapeutic target for the treatment of several types of tumors.[46–48] Furthermore, cyclin D1 and cyclin D3 are the major players for G1 to S transition,[49,50] and it is tempting to speculate that the observed cell-cycle arrest upon RMC-6272 treatment may—at least in part—be due to decreases in these cell-cycle regulators. However, further studies are needed to elucidate the broader spectrum of translational changes that may be responsible for cell-cycle arrest and/or the anti-proliferative activity observed upon RMC-6272 treatment.

In addition to our 2D in vitro studies, we further examined the effects of RMC-6272 in a 3D multicellular spheroid model as well as in vivo mouse models of meningioma. Here, we have established a reproducible, cost-effective, and scalable protocol for generating *NF2*-deficient meningioma spheroids and evaluated 3 classes of mTOR inhibitors. Similar to 2D cultures, we found RMC-6272 to be superior to both first- and second-generation mTOR inhibitors in 3D spheroids from grade I and grade III meningiomas. We have also observed a significant reduction in schwannoma spheroid size upon RMC-6272 treatment. It is noteworthy that a 100-fold increase in the concentration of INK128 was required to achieve a similar level of reduction in meningioma spheroid area compared with RMC-6272. Importantly, meningioma-bearing mice treated with RMC-6272 at 3 and 8 mg/kg did not show any overt weight loss and these treatments led to significant reduction in tumor growth in 2 intracranial meningioma xenograft models.

Taken together, our study demonstrates that RMC-6272 is mTORC1-selective, inhibiting both S6K and 4E-BP1 with a longer retention time, effectively reduces global translation and potently inhibits meningioma growth both in vitro and in vivo. These data highlight the importance of mTORC1–4E-BP1–eIF4E signaling in NF2-related tumors and raise the possibility that targeting 5′cap-dependent translation may be a more effective therapeutic approach for *NF2*-deficient tumors. Additionally, here we show the generation of 3D spheroids from *NF2*-deficient meningioma and schwannoma cell lines as a complementary approach to traditional 2D in vitro and in vivo mouse models, which can serve as an important tool for future NF2 studies. Our results suggest that more complete inhibition of mTORC1 signaling may enhance antitumor activity and provide a compelling basis for potential future clinical evaluation of bi-steric mTORC1 inhibitors, either alone or in combination with other drugs for NF2 and sporadic tumors with *NF2* loss.

Supplementary material

Supplementary material is available online at *Neuro-Oncology Advances* (https://academic.oup.com/noa).

Keywords

4E-BP1 | meningioma | mTORC1 | NF2 | RMC-6272

Funding

This study was supported by the National Institutes of Health (R01 NS113854 to V.R.) and Department of Defense (W81XWH-18-1-0547 to L.-S.C.).

Acknowledgments

We would like to sincerely acknowledge our valuable discussions with Dr. Jerry Pelletier from the Goodman Cancer Research Institute at McGill University, Montreal, Canada, who unfortunately passed away during the completion of this study. We thank Jacob Brenner for technical assistance and Revolution Medicines, Inc., for providing RMC-6272 for this study. The schematics have been created using Biorender.com.

Conflict of interest statement

The authors declare that no conflicts of interest exist.

Authorship statement

Experimental design: S.B., J.L.O., R.L.B., F.R., L.-S.C., and V.R. Implementation: S.B., J.L.O., R.L.B., F.R., L.K., and L.-S.C. Analysis or interpretation of data: S.B., J.L.O., R.L.B., F.R., L.K., S.R.P., L.-S.C., and V.R. Manuscript writing/review: all authors.

Data availability

Relevant data will be made available upon reasonable request.

Affiliations

Department of Neurology and Center for Genomic Medicine, Massachusetts General Hospital, Boston, Massachusetts, USA (S.B., R.L.B., L.K., V.R.); Cancer Center, Massachusetts General Hospital, Boston, Massachusetts, USA (S.R.P.); Center for Childhood Cancer, Nationwide Children's Hospital and Department of Pediatrics, The Ohio State University College of Medicine, Columbus, Ohio, USA (J.L.O., L.-S.C.); Department of Biochemistry and Goodman Cancer Research Institute, McGill University, Montreal, Quebec, Canada (F.R.)

References

1. Baser ME; Contributors to the International NF2 Mutation Database. The distribution of constitutional and somatic mutations in the neurofibromatosis 2 gene. *Hum Mutat.* 2006;27(4):297–306.
2. Jordan JT, Orr CC, Thalheimer RD, et al. Prospective phase II trial of the dual mTORC1/2 inhibitor vistusertib for progressive or symptomatic meningiomas in persons with neurofibromatosis 2. *Neurooncol Adv.* 2023;5(1):vdad041.

3. Coy S, Rashid R, Stemmer-Rachamimov A, Santagata S. An update on the CNS manifestations of neurofibromatosis type 2. *Acta Neuropathol.* 2020;139(4):643–665.
4. Wang JZ, Nassiri F, Mawrin C, Zadeh G. Genomic landscape of meningiomas. In: Zadeh G, Goldbrunner R, Krischek B, Nassiri F, eds. *Biological and Clinical Landscape of Meningiomas.* Advances in Experimental Medicine and Biology. Vol. 1416. Cham: Springer; 2023:137–158.
5. Vagnoni L, Aburas S, Giraffa M, et al. Radiation therapy for atypical and anaplastic meningiomas: an overview of current results and controversial issues. *Neurosurg Rev.* 2022;45(5):3019–3033.
6. Choudhury A, Chen WC, Lucas CG, et al. Hypermitotic meningiomas harbor DNA methylation subgroups with distinct biological and clinical features. *Neuro Oncol.* 2023;25(3):520–530.
7. Blakeley JO, Evans DG, Adler J, et al. Consensus recommendations for current treatments and accelerating clinical trials for patients with neurofibromatosis type 2. *Am J Med Genet A.* 2012;158A(1):24–41.
8. James MF, Lelke JM, Maccollin M, et al. Modeling NF2 with human arachnoidal and meningioma cell culture systems: NF2 silencing reflects the benign character of tumor growth. *Neurobiol Dis.* 2008;29(2):278–292.
9. James MF, Han S, Polizzano C, et al. NF2/merlin is a novel negative regulator of mTOR complex 1, and activation of mTORC1 is associated with meningioma and schwannoma growth. *Mol Cell Biol.* 2009;29(15):4250–4261.
10. Goutagny S, Giovannini M, Kalamarides M. A 4-year phase II study of everolimus in NF2 patients with growing vestibular schwannomas. *J Neurooncol.* 2017;133(2):443–445.
11. Goutagny S, Raymond E, Esposito-Farese M, et al. Phase II study of mTORC1 inhibition by everolimus in neurofibromatosis type 2 patients with growing vestibular schwannomas. *J Neurooncol.* 2015;122(2):313–320.
12. Giovannini M, Bonne NX, Vitte J, et al. mTORC1 inhibition delays growth of neurofibromatosis type 2 schwannoma. *Neuro Oncol.* 2014;16(4):493–504.
13. Choo AY, Yoon SO, Kim SG, Roux PP, Blenis J. Rapamycin differentially inhibits S6Ks and 4E-BP1 to mediate cell-type-specific repression of mRNA translation. *Proc Natl Acad Sci U S A.* 2008;105(45):17414–17419.
14. Lee BJ, Boyer JA, Burnett GL, et al. Selective inhibitors of mTORC1 activate 4EBP1 and suppress tumor growth. *Nat Chem Biol.* 2021;17(10):1065–1074.
15. Beauchamp RL, James MF, DeSouza PA, et al. A high-throughput kinome screen reveals serum/glucocorticoid-regulated kinase 1 as a therapeutic target for NF2-deficient meningiomas. *Oncotarget.* 2015;6(19):16981–16997.
16. James MF, Stivison E, Beauchamp R, et al. Regulation of mTOR complex 2 signaling in neurofibromatosis 2-deficient target cell types. *Mol Cancer Res.* 2012;10(5):649–659.
17. Hagiwara A, Cornu M, Cybulski N, et al. Hepatic mTORC2 activates glycolysis and lipogenesis through Akt, glucokinase, and SREBP1c. *Cell Metab.* 2012;15(5):725–738.
18. Meng D, Zhao X, Yang YC, et al. A bi-steric mTORC1-selective inhibitor overcomes drug resistance in breast cancer. *Oncogene.* 2023;42(28):2207–2217.
19. Rodrik-Outmezguine VS, Okaniwa M, Yao Z, et al. Overcoming mTOR resistance mutations with a new-generation mTOR inhibitor. *Nature.* 2016;534(7606):272–276.
20. Burnett GL, Yang YC, Aggen JB, et al. Discovery of RMC-5552, a selective bi-steric inhibitor of mTORC1, for the treatment of mTORC1-activated tumors. *J Med Chem.* 2023;66(1):149–169.
21. Morales J, Allegakoen DV, Garcia JA, et al. GATOR2-dependent mTORC1 activity is a therapeutic vulnerability in FOXO1 fusion-positive rhabdomyosarcoma. *JCI Insight.* 2022;7(23):e162207.
22. Lee BJ, Mallya S, Dinglasan N, et al. Efficacy of a novel bi-steric mTORC1 inhibitor in models of B-cell acute lymphoblastic leukemia. *Front Oncol.* 2021;11(Aug 2):673213.
23. Puttmann S, Senner V, Braune S, et al. Establishment of a benign meningioma cell line by hTERT-mediated immortalization. *Lab Invest.* 2005;85(9):1163–1171.
24. Beauchamp RL, Erdin S, Witt L, et al. mTOR kinase inhibition disrupts neuregulin 1-ERBB3 autocrine signaling and sensitizes NF2-deficient meningioma cellular models to IGF1R inhibition. *J Biol Chem.* 2021;296(Jan-June):100157.
25. Tanaka K, Sato C, Maeda Y, et al. Establishment of a human malignant meningioma cell line with amplified c-myc oncogene. *Cancer.* 1989;64(11):2243–2249.
26. Burns SS, Akhmametyeva EM, Oblinger JL, et al. Histone deacetylase inhibitor AR-42 differentially affects cell-cycle transit in meningeal and meningioma cells, potently inhibiting NF2-deficient meningioma growth. *Cancer Res.* 2013;73(2):792–803.
27. Sagers JE, Beauchamp RL, Zhang Y, et al. Combination therapy with mTOR kinase inhibitor and dasatinib as a novel therapeutic strategy for vestibular schwannoma. *Sci Rep.* 2020;10(1):4211.
28. Wiederhold T, Lee MF, James M, et al. Magicin, a novel cytoskeletal protein associates with the NF2 tumor suppressor merlin and Grb2. *Oncogene.* 2004;23(54):8815–8825.
29. Bhattacharyya S, Oblinger JL, Beauchamp RL, et al. Proteasomal pathway inhibition as a potential therapy for NF2-associated meningioma and schwannoma. *Neuro Oncol.* 2023;25(9):1617–1630.
30. Tofani LB, Abriata JP, Luiz MT, Marchetti JM, Swiech K. Establishment and characterization of an in vitro 3D ovarian cancer model for drug screening assays. *Biotechnol Prog.* 2020;36(6):e3034.
31. Tofani LB, Sousa LO, Luiz MT, et al. Generation of a three-dimensional in vitro ovarian cancer co-culture model for drug screening assays. *J Pharm Sci.* 2021;110(7):2629–2636.
32. Bhattacharyya S, Ghosh SS. Transmembrane TNFalpha-expressed macrophage membrane-coated chitosan nanoparticles as cancer therapeutics. *ACS Omega.* 2020;5(3):1572–1580.
33. Enot DP, Vacchelli E, Jacquelot N, Zitvogel L, Kroemer GT. An open-access web tool for the statistical analysis of tumor growth curves. *Oncoimmunology.* 2018;7(9):e1462431.
34. Fan Q, Aksoy O, Wong RA, et al. A kinase inhibitor targeted to mtorc1 drives regression in glioblastoma. *Cancer Cell.* 2017;31(3):424–435.
35. Romagnoli A, D'Agostino M, Ardiccioni C, et al. Control of the eIF4E activity: structural insights and pharmacological implications. *Cell Mol Life Sci.* 2021;78(21–22):6869–6885.
36. Uttam S, Wong C, Price TJ, Khoutorsky A. eIF4E-dependent translational control: a central mechanism for regulation of pain plasticity. *Front Genet.* 2018;9(Oct 24):470.
37. Fennema E, Rivron N, Rouwkema J, van Blitterswijk C, de Boer J. Spheroid culture as a tool for creating 3D complex tissues. *Trends Biotechnol.* 2013;31(2):108–115.
38. Breslin S, O'Driscoll L. Three-dimensional cell culture: the missing link in drug discovery. *Drug Discov Today.* 2013;18(5–6):240–249.
39. Pampaloni F, Reynaud EG, Stelzer EH. The third dimension bridges the gap between cell culture and live tissue. *Nat Rev Mol Cell Biol.* 2007;8(10):839–845.
40. van de Weijer LL, Ercolano E, Zhang T, et al. A novel patient-derived meningioma spheroid model as a tool to study and treat epithelial-to-mesenchymal transition (EMT) in meningiomas. *Acta Neuropathol Commun.* 2023;11(1):198.
41. Pinto B, Henriques AC, Silva PMA, Bousbaa H. Three-dimensional spheroids as in vitro preclinical models for cancer research. *Pharmaceutics.* 2020;12(12):1186.
42. Zhou Y. The application of ultrasound in 3D bio-printing. *Molecules.* 2016;21(5).
43. Kuroshima K, Yoshino H, Okamura S, et al. Potential new therapy of Rapalink-1, a new generation mammalian target of rapamycin

inhibitor, against sunitinib-resistant renal cell carcinoma. *Cancer Sci*. 2020;111(5):1607–1618.

44. Vargas-Toscano A, Nickel AC, Li G, et al. Rapalink-1 targets glioblastoma stem cells and acts synergistically with tumor treating fields to reduce resistance against temozolomide. *Cancers (Basel)*. 2020;12(12):3859.
45. Du H, Yang YC, Liu HJ, et al. Bi-steric mTORC1 inhibitors induce apoptotic cell death in tumor models with hyperactivated mTORC1. *J Clin Invest*. 2023;133(21):e167861.
46. Ma H, Li Q, Wang J, et al. Dual inhibition of ornithine decarboxylase and a(1) adenosine receptor efficiently suppresses breast tumor cells. *Front Oncol*. 2021;11(Mar 11):636373.
47. Elmets CA, Athar M. Targeting ornithine decarboxylase for the prevention of nonmelanoma skin cancer in humans. *Cancer Prev Res (Phila)*. 2010;3(1):8–11.
48. He W, Roh E, Yao K, et al. Targeting ornithine decarboxylase (ODC) inhibits esophageal squamous cell carcinoma progression. *npj Precis Oncol*. 2017;1(1):13.
49. Montalto FI, De Amicis F. Cyclin D1 in cancer: a molecular connection for cell cycle control, adhesion and invasion in tumor and stroma. *Cells*. 2020;9(12):2648.
50. Sawai CM, Freund J, Oh P, et al. Therapeutic targeting of the cyclin D3:CDK4/6 complex in T cell leukemia. *Cancer Cell*. 2012;22(4):452–465.